Pergamon

J. Mech. Phys. Solids, Vol. 44, No. 2, pp. 179–205, 1996

0022–5096/96 $15.00 + 0.00

0022–5096(95)00075–5

MODELING OF HYDROGEN TRANSPORT AND ELASTICALLY ACCOMMODATED HYDRIDE FORMATION NEAR A CRACK TIP

J. LUFRANO,† P. SOFRONIS†* and H. K. BIRNBAUM‡

Departments of †Theoretical and Applied Mechanics and ‡Materials Science and Engineering, University of Illinois at Urbana-Champaign, Urbana, IL 61801, U.S.A.

(*Received* 7 *June* 1995; *in revised form* 20 *September* 1995)

ABSTRACT

Transient hydrogen diffusion and elastically accommodated hydride formation coupled with material elastic deformation are studied in a hydride forming system. The constitutive behavior of the material is modeled as isotropically linear elastic and account is taken of the effect of the dilatational strain induced by the solute hydrogen and formed hydride. The concept of terminal solid solubility of hydrogen as affected by stress is described and the mode of hydrogen diffusion through the two-phase material (matrix + hydride) is discussed. Probabilistic precipitation of hydride is modeled in the neighborhood of a stationary sharp crack tip under mode I plane strain loading, fixed hydrogen concentration on the crack surfaces and the outer boundary, and a uniform initial hydrogen concentration below the stress-free terminal solid solubility. A full transient finite element analysis allows for numerical monitoring of the development and expansion of the hydride zone. Information about the shape, size and density of the hydride in the hydride zone is obtained. The mechanistic effects of the solute hydrogen and hydride formation on the stress intensity at the crack tip are analyzed and their consequence on the fracture toughness resistance of the material is discussed.

1. INTRODUCTION

Hydrogen embrittlement, a severe degradation of the mechanical properties of materials in the presence of hydrogen, is governed by complex multiple mechanisms. Even in specific materials the embrittling mechanisms are not well established (Birnbaum, 1979, 1983, 1984; Birnbaum and Sofronis, 1994). One useful classification is to distinguish between systems which form hydrides and those which do not form hydrides under the relevant hydrogen fugacity and applied stress.

The present study is concerned with hydride forming systems. A number of authors (Takano and Suzuki, 1974; Birnbaum *et al.*, 1976; Gahr *et al.*, 1977; Grossbeck and Birnbaum, 1977; Shih *et al.*, 1988) have shown that embrittlement occurs by hydride formation at severe stress raisers such as crack tips followed by cleavage of the brittle hydride (Westlake, 1969). The phenomenon is intermittent, with the crack propagating through the hydride and stopping when it reaches the matrix.

* To whom all correspondence should be addressed.

Subsequently, new hydride forms either autocatalytically (Shih *et al.*, 1988) or as a result of external loading, and then cleavage reinitiates (Westlake, 1969). Stress induced hydride formation is a consequence of the volume dilatation, of the order of 15% which accompanies hydride precipitation (Westlake, 1969; Birnbaum *et al.*, 1976; Gahr *et al.*, 1977; Grossbeck and Birnbaum, 1977; Flanagan *et al.*, 1981; Puls, 1984). It has been experimentally shown (Gahr *et al.*, 1977; Grossbeck and Birnbaum, 1977) that hydrides form in regions of hydrostatic tensile stress even at temperatures which are above the solvus temperature in the absence of stress. The hydride formation is a result of the enhanced hydrogen concentration in the area of tensile stress (Li *et al.*, 1966) and the decreased chemical potential of the hydride relative to the solid solution in the same stress field (Birnbaum *et al.*, 1976; Gahr *et al.*, 1977; Grossbeck and Birnbaum, 1977; Flanagan *et al.*, 1981; Puls, 1984).

In brittle materials the stress intensity at crack tips has been shown to be changed by phase transformation which is accompanied by volume dilatation (McMeeking and Evans, 1982; Budiansky *et al.*, 1983). Substantial effects of crack tip shielding resulting from phase transformation were found for dilatations of the order of 1% in zones extending approximately 10 microns on either side of a substantially advanced crack (McMeeking and Evans, 1982). Hence, the precipitated hydrides may mechanically influence the crack tip stress (Hirth, 1987) in addition to the material degradation which results from the hydride's extremely brittle nature (Gahr *et al.*, 1977, 1980; Simpson and Puls, 1979). Some evidence for crack tip shielding as a result of the presence of hydrides has been seen in α titanium (Shih *et al.*, 1988) and zirconium (Simpson and Puls, 1979).

Mathematical modeling of these phenomena was first carried out (Dutton *et al.*, 1977) by modeling the steady state hydride precipitation at a crack tip and by solving the one-dimensional diffusion equation accounting for the hydrostatic stress gradient drift. The average growth rate of the hydride was computed and the crack velocity was equated with the hydride growth rate. Similar treatments have been given by a number of other authors (Dutton and Puls, 1976; Dutton *et al.*, 1978; Simpson and Puls, 1979; White *et al.*, 1985, Shalabi and Meneley, 1991). Ellyin and Wu (1994) modeled the hydride effect on the elastoplastic stress field near a crack tip but the coupled hydrogen diffusion and mechanics phenomena were not treated. More recently, Shi *et al.* (1994) extended the model of Dutton and Puls (1976) to non-steady state conditions in zirconium alloys. The model is a one-dimensional treatment of hydrogen diffusion at a crack tip in which the hydride forms in the unperturbed stress field of a crack and grows only along the axis of symmetry directly ahead of the tip, while its thickness remains constant. The model results indicate that the hydride length increases rapidly with time at first, but eventually reaches a limit which increases with bulk hydrogen concentration and applied load. Also at low stress intensities, the model indicates a threshold behavior in hydride cracking which is dependent on the hydrogen concentration in the bulk.

The phenomenology of hydrogen embrittlement in hydride forming systems will be better understood if realistic and precise modeling of the mechanics of hydride formation and fracture is available. The primary focus of this paper is to model the stress induced hydrogen transport and hydride formation in the vicinity of a stationary crack with use of a continuum mechanics approach. It is well established that the

solutions to the hydrogen diffusion and hydride precipitation problems are intimately coupled to the solution of the elastoplastic boundary value problem (Birnbaum *et al.*, 1976; Sofronis, 1987; Sofronis and McMeeking, 1989). In this work, however, the hydride precipitation will be modeled in an elastically accommodating matrix to simplify the numerical calculations. As will be discussed, plastic accommodation of the volume change which accompanies hydride formation decreases the "effective elastic volume change for hydride formation" and hence makes the solvus temperature less sensitive to applied stresses. This effect can be modeled by choosing the appropriate change in volume on forming a hydride from the solid solution. The most important effect of plastic accommodation is on the kinetics of crack propagation since the presence of plastic accommodation inhibits resolution of the stress stabilized hydride once the external stress is removed. Thus in the presence of solely elastic accommodation, the hydrides formed at the crack tip will redissolve as the crack propagates (Takano and Suzuki, 1974) and serve as a source of hydrogen for the new stress stabilized hydrides at the advanced crack tip position. When the hydrides are plastically accommodated, resolution of the hydrides is inhibited by the reverse plastic accommodation required on resolution (Birnbaum *et al.*, 1976). In this case the hydrides left in the wake of the advancing crack will not redissolve and hydrogen for the new crack tip hydrides must be supplied by diffusion from the far field regions of the diffusion field. The present model discusses the kinetics of hydride formation in front of a stationary crack and consequently applies to both systems which exhibit purely elastic accommodation, e.g. vanadium (Takano and Suzuki, 1974) and the more frequent case of systems which have both elastic and plastic accommodation of the hydrides (where an "effective elastic volume change on hydride formation" would replace the actual volume change). A detailed treatment of the crack propagation kinetics in the presence of plastic accommodation of the hydrides and plasticity at the crack tip will be presented in a subsequent paper. Apart from the idealized condition of elastic accommodation, care is taken so that the assumptions used are physically based and result in realistic modeling. Full transient analysis allows for the monitoring of the size, shape and density of the developing hydride zone. Calculations are made to determine the effect of the hydrides on the stress field and the local stress intensity factor at the crack tip. The results are used to quantitatively address the mechanistic effects of hydride growth on fracture behavior in hydride forming systems.

2. STRESS INDUCED HYDROGEN TRANSPORT AND HYDRIDE FORMATION

The terminal solid solubility (TSS), also termed the solvus concentration, of hydrogen in solution in metal under external stress, σ_{ij}, is given by (Birnbaum *et al.*, 1976; Grossbeck and Birnbaum, 1977; Gahr and Birnbaum, 1978; Flanagan *et al.*, 1981; Puls, 1981, 1984)

$$c_s^\sigma = A \exp\left(\frac{H_h}{RT}\right) \exp\left(\frac{W_{acc}}{RT}\right) \exp\left(\frac{W_{int}}{RT}\right), \tag{1}$$

where c_s^σ is the solvus concentration (hydrogen atoms per solution atom) in equilibrium with the hydride phase at temperature, T, and stress, σ_{ij}, A is a constant, W_{acc} denotes the accommodation Gibbs free energy change per mole of hydride, i.e. the free energy of elastically and plastically accommodating the transformation strain on forming the hydride from the solid solution, W_{int} denotes the interaction Gibbs free energy per mole of hydride of the externally applied stress and the transformation strain that accommodates the hydride formation, and R is the gas constant. The parameter H_h is the molal enthalpy change for transferring hydrogen from the solid solution to the hydride in the absence of any accommodation stress or the external stress. For the hydride forming systems $H_h < 0$. The stress-free terminal solid solubility, i.e. that which characterizes the equilibrium between the solid solution and an unconfined hydride is characterized by H_h, a parameter which cannot be easily measured. The value of H_h is approximated by the temperature dependence of the solid solubility measured on heating (Birnbaum *et al.*, 1976).

In an elastically deforming matrix the energy of accommodation, W_{acc}, is a purely elastic energy

$$W_e = -\frac{1}{2}\int_V \sigma_{ij}^I \varepsilon_{ij}^T \, dV, \tag{2}$$

where σ_{ij}^I is the stress in the constrained hydride, ε_{ij}^T is the total transformation strain in going from a solid solution to the hydride, and V is the volume occupied by a mole of hydride (Eshelby, 1956, 1957). Note that while the solid solution–hydride surface energy should also be considered, it is small compared to W_e.

In general, the matrix cannot accommodate the large transformation strains elastically and a part of the accommodation is by plastic deformation (Birnbaum *et al.*, 1976). The free energy term, W_{acc}, therefore contains both elastic and plastic energy terms, $W_{acc} = W_{el} + W_{pl}$. The elastic accommodation strain, $(\varepsilon_{ij}^{el})^T$, corresponds, in this case, to the part of the total volume change which is elastically accommodated and the plastic accommodation energy, W_{pl}, is associated with the plastic accommodation strains, $(\varepsilon_{ij}^{pl})^T = \varepsilon_{ij}^T - (\varepsilon_{ij}^{el})^T$. While calculation of W_{pl} is model dependent, in general $W_{acc} \approx W_{el}$ where the elastic accommodation energy is calculated as in (2), $W_{el} = W_e$, using the full hydride transformation strain.

In addition to the accommodation free energy terms, the volume expansion results in a free energy term due to the applied stress which in the case of elastically accommodated hydride is given by

$$W_{int} = -\int_V \sigma_{ij} \varepsilon_{ij}^T \, dV, \tag{3}$$

where σ_{ij} is the stress caused by the externally applied loads and V is the volume occupied by a mole of hydride (Eshelby, 1956, 1957). For a uniformly applied stress, the transformation strain to be considered is that of the solid solution transforming to a hydride at the same composition, MH, i.e. 1 mole each of metal, M, and hydrogen, H. In the case of purely dilatational transformation

$$W_{\text{int}} = -\frac{\sigma_{kk}}{3}(V_{\text{h}} - V_{\text{H}}), \tag{4}$$

where V_{H} is the partial molar volume of hydrogen in solid solution and V_{h} is the partial molar volume of hydrogen in the hydride. Note that $V_{\text{h}} - V_{\text{H}}$ denotes the local volume change associated with the transfer of a mole of hydrogen from solution to hydride.

The situation is rather different in the presence of an inhomogeneous stress field such as near a crack tip (Flanagan *et al.*, 1981) where the hydride and solid solution molar free energies differ in the highly stressed element of volume and the low stressed element of volume. In this case of inhomogeneous stress, which is relevant to the situation considered in the present paper, the appropriate transformation strain is that of a solid solution of composition MH_a, where a is the number of hydrogen atoms per metal atom and is typically less than one, transforming to the hydride MH, with a requirement for additional H which must come from a low stress element of volume. Considering only dilatational strains

$$W_{\text{int}} = -\frac{\sigma_{kk}}{3}(V_{\text{hr}} - V_{\text{s}}) \tag{5}$$

or equivalently

$$W_{\text{int}} = -\frac{\sigma_{\text{kk}}}{3(1-a)}(V_{\text{hr}} - (V_{\text{M}} + aV_{\text{H}})), \tag{6}$$

where V_{hr} is the molar volume of MH hydride, V_{s} is the molar volume of the solid solution MH_a having the hydrogen concentration $H/M = a$ and V_{M} is the partial molar volume of the metal. Due to the large composition change $(V_{\text{hr}} - V_{\text{s}}) > (V_{\text{h}} - V_{\text{H}})$, and the stress effects on the hydride are largest at elastic singularities. In the present calculation, the transformation strain associated with the hydride formation is assumed to be purely dilatational. While this is a good approximation, there are non-zero shear strain components, since in general the symmetry of the hydride differs from that of the solid solution.

To model hydrogen transport it is assumed that solute hydrogen resides in normal interstitial lattice sites in a continuous distribution throughout the lattice allowing a continuum description for the solid solution material to be formulated (Sofronis and Birnbaum, 1995). In this purely elastic calculation, trapping of hydrogen at microstructural defects is not considered. Disregard of trapping of hydrogen by lattice defects does not seriously affect the result in the case of the elastic calculation as the defect trap concentration is sufficiently low to allow local equilibrium between the solute hydrogen and the defect traps. Hydrogen moves through the lattice by interstitial diffusion and its mobility is very high in the temperature range in which hydride embrittlement is observed (Völkl and Alefeld, 1978). The diffusivity in solid solutions in metal is much higher than in those hydrides in which hydrogen diffusion has been measured. Hence, in the present study, the dominant mode for diffusion is through the metal solid solution. Dislocation transport (Tien *et al.*, 1981) is not considered to

be significant, in agreement with recent observations (Frankel and Latanision, 1986; Ladna and Birnbaum, 1987).

The driving force for hydrogen diffusion in the lattice are chemical potential gradients, which are naturally present in the vicinity of a crack tip. Volume dilatation caused by the dissolved hydrogen results in a decrease in the chemical potential of hydrogen in solid solution when a tensile stress (uniaxial or hydrostatic) is applied. This effect can be described by

$$\mu_\sigma - \mu_0 = -\frac{\sigma_{kk}}{3} V_H, \tag{7}$$

where μ_σ is the chemical potential in the stressed region and μ_0 is the chemical potential in the unstressed volume. A system in which the stress state is not homogeneous, such as at the tip of the crack, the hydrogen concentration will increase in the regions of the highest tensile stress until the chemical potential gradient caused by the applied stress is removed.

Hydride precipitation results from the effect of the stress on both the hydrogen concentration in solid solution and on the hydride solvus, with the later effect dominating. When a tensile stress is applied to the solid solution, hydrogen diffusion to regions of highest tensile hydrostatic stress will occur, i.e. to the elastic singularity at the crack tip. As a result the local concentrations of hydrogen are increased until the stress driven chemical potential gradients are removed. This factor by itself would not cause hydride precipitation. However, the chemical potential of the hydride phase in the hydrostatic stress field of the elastic singularity is decreased by the applied stress leading to a decrease in the local solvus concentration as given by (1). Hydride is then formed at the crack tip. Due to the high hydrogen diffusivity, local equilibrium is rapidly achieved by hydrogen diffusion toward the crack tip with the hydride approaching the composition MH and the adjacent solid solution maintaining the composition c_s^σ. The flux of hydrogen to the growing hydride is driven by the concentration gradient, $c_s^\sigma < c_s$, where c_s denotes the hydrogen concentration far from the crack tip expressed in hydrogen atoms per solid solution atom, and by the effect of stress on the chemical potential of hydrogen in solid solution.

Hydride growth will continue until the free energy of the system achieves a minimum. In a closed system hydride precipitation occurs until $c_s = c_s^\sigma$, while in an open system hydrogen can enter the system until hydride occupies the entire volume. A number of possible modes of hydride growth can be considered. One possibility is that since the accommodation free energy increases as the hydride grows, massive hydride will grow in the triaxial stress field until its growth is stopped by the accumulation of plastic accommodation free energy. Alternatively, plate-like hydrides can form and these generate a stress field at their edges which is similar to wedge-opening mode I cracks (Shih *et al.*, 1988). Under these conditions the plates will grow out of the crack tip stress field with their growth sustained by the stress field at the hydride (autocatalytic growth) (Shih *et al.*, 1988).

Finally, it should be emphasized that the prediction of hydride formation in the present treatment is probabilistic in nature. The tendency of hydrides to grow in platelet-like shapes and the effect of hydride shape on subsequent precipitation is not considered in the present calculation.

3. THE INITIAL BOUNDARY VALUE PROBLEM

3.1. *Formulation of the hydrogen diffusion initial boundary value problem allowing for hydride formation*

Let C_L denote the hydrogen concentration in the lattice expressed as hydrogen atoms per unit volume of solid solution phase when the hydride volume fraction f is less than one. At a given time t with the composition of the composite defined pointwise by its hydride volume fraction f such that $0 \leqslant f \leqslant 1$, the hydrogen diffusion equation (Sofronis, 1987; Sofronis and McMeeking, 1989) is written as follows

$$Q\frac{\partial C_L}{\partial t} = \left(D_c C_{L,i} + \frac{D_c C_L}{RT}\mu_{\sigma,i}\right)_{,i}, \tag{8}$$

where $(\,)_{,i} = \partial(\,)/\partial x_i$, $\mathrm{d}/\mathrm{d}t$ denotes differentiation with respect to time, Q is given as

$$Q = \begin{cases} 1-f & \text{if} \quad 0 \leqslant f < 1 \\ 1 & \text{if} \quad f = 1 \end{cases}, \tag{9}$$

D_c is an effective diffusion constant for the hydrogen diffusing through the composite material given by

$$D_c = \begin{cases} (1-f)D_s & \text{if} \quad 0 \leqslant f < 1 \\ D_h & \text{if} \quad f = 1 \end{cases}, \tag{10}$$

where D_s and D_h represent the diffusion constants of hydrogen in solution with metal and in the hydride, respectively. The parameter μ_σ is the stress dependent part of the chemical potential of hydrogen in solution and is given by (7) and only dilatational distortion of the lattice is considered. It should be emphasized that μ_σ as used in (6) and (8) also may be used to represent the effect of stress on the chemical potential of the hydrogen in the hydride which is in equilibrium with the solid solution. This is approximately correct as $V_H \approx V_h$ for most systems. In the niobium–hydrogen system $V_h \approx 1.03 V_H$ (Hindin and Birnbaum, 1981).

Solution of the governing equation (8) at any time t with given hydride volume fraction f_t furnishes the pointwise concentration, C_L. In regions where $0 \leqslant f < 1$, one can write

$$C_L = \frac{c_s}{1-c_s}\frac{N_A}{V_M}, \tag{11}$$

where c_s denotes hydrogen atoms per solid solution atom, N_A is Avogadro's number and V_M is the molar volume of metal M. In any infinitesimal volume, the concentration c_s, as computed by (11), determines whether hydride precipitation f' occurs in the part $1-f_t$ of the volume which is still solid solution. The volume fraction f' is such that $0 \leqslant f' < 1$ and is used to define parameter f at time $t+\Delta t$ as

$$f_{t+\Delta t} = f_t + f'(1-f_t). \tag{12}$$

This amounts to a forward Euler algorithm that is carried out as follows

$$f' = \begin{cases} 0 & \text{if} \quad c_s < c_s^\sigma \\ f_l & \text{if} \quad c_s^\sigma \leqslant c_s < c_h \\ 1 & \text{if} \quad c_h \leqslant c_s \end{cases} \tag{13}$$

where c_h is the concentration above which the whole lattice turns into hydride. It equals 0.5 for the assumed hydride composition MH. In (13) the parameter f_l is determined by means of the lever rule and is given as

$$f_l = \frac{1}{1 + \dfrac{(1-c_s^\sigma)(1-2c_s)V_M}{(c_s - c_s^\sigma)V_{hr}}}, \tag{14}$$

where it should be recalled that c_s^σ is sensitive to the hydrostatic stress as described by (1). Lastly, adjustment of the concentration C_L furnishes the concentration at time $t+\Delta t$

$$(C_L)_{t+\Delta t} = \begin{cases} C_L & \text{if} \quad f' = 0 \\ C_{LS} & \text{if} \quad 0 < f' < 1, \\ C_{hs} & \text{if} \quad f' = 1 \end{cases} \tag{15}$$

where C_{LS} is given by (11) for $c_s = c_s^\sigma$. The concentration C_{hs} denotes hydrogen atoms in solution with the hydride per unit volume of composite material and is given by

$$C_{hs} = (C_L - C_{Lh})(1 - f_l), \tag{16}$$

where C_{Lh} is given by (11) for $c_s = c_h$. Note that in this case, $f' = 1$, and the local volume is 100% hydride.

3.2. *Formulation of the elasticity boundary value problem*

In the present section the hydride formation is considered in relationship to the mechanical behavior of the hydride–solid solution composite. This work considers the situation where hydride forms at stresses lower than the yield stress. In this case, the hydride zones occupy the regions which otherwise would be plastic zones in front of the crack tip. While it should be noted that other situations can arise (Birnbaum, 1984), the case chosen for analysis is the simplest to model. The hydride zone is considered to be purely elastic and any plastic accommodation is neglected.

At any stage of loading, the transformation strain rate due to hydride formation and the presence of solute hydrogen is assumed to be purely dilational and is given by

$$\dot{\varepsilon}_{ij}^T = \frac{1}{3}\frac{d}{dt}\left[f\theta_{hr} + (1-f)\frac{c_s}{1-c_s}\theta_h\right]\delta_{ij}, \tag{17}$$

where $\dot{(\ )} = d(\ )/dt$, δ_{ij} is the Kronecker delta, θ_{hr} is the volume dilatation of a composite material element that is 100% hydride compared to the solid solution, and θ_h is the lattice induced local dilatation when hydrogen dissolves in solution with the metal (Peisl, 1978).

The material is assumed to be isotropic and the corresponding linear elastic relationship has the form

$$\sigma_{ij} = 2G\varepsilon'_{ij} + B(\varepsilon_{kk} - \varepsilon^{T}_{kk})\delta_{ij}, \tag{18}$$

where ε_{ij} is the deviatoric part of the strain, $\varepsilon_{ij} = (\partial u_i/\partial x_j + \partial u_j/\partial x_i)/2$, u_i is the displacement, and G and B are the shear and bulk moduli, respectively, which are assumed unperturbed by the presence of solute hydrogen and hydride. In the absence of body forces the governing equations of rate equilibrium are written in the form of the principle of virtual velocities

$$\int_V \dot{\sigma}_{ij}\delta\dot{\varepsilon}_{ij}\,\mathrm{d}V = \int_S \dot{T}_i\delta v_i\,\mathrm{d}S, \tag{19}$$

where V is the volume bounded by the surface S, T_i are the components of the traction vector which is specified on the part S_T of the surface where tractions are prescribed, v_i are the components of the velocity, $v_i = \dot{u}_i$, which is prescribed on the part $S - S_T$ of the surface where S is the total surface. Any virtual velocity variations vanish on $S - S_T$. Equation (19) is non-linear because the stress rate $\dot{\sigma}_{ij}$ depends on $\dot{f}$ which has to be determined in conjunction with the hydrogen diffusion problem. The situation represents an elasticity problem coupled to stress controlled transformation and diffusion.

3.3. *Small scale hydride formation at a crack tip*

The analysis is carried out in a material with a mathematically sharp crack (see Fig. 1) lying along $x_1 < 0$ and having its surfaces on $\theta = \pm\pi$. The elastic boundary value problem is analyzed in plane strain mode I loading conditions. The loading is carefully monitored to ensure that the zones of hydride and hydrogen-enriched material have a maximum distance from the crack tip which is small compared to the distance to the outer boundary (Lufrano and Sofronis, 1995). As a consequence, the problem can be studied by following the boundary layer approach (Rice, 1968), namely by imposing tractions on a circular boundary far from the tip (see Fig. 1) in agreement with the standard singular linear elastic solution given by

$$T_i = \frac{K_A}{\sqrt{2\pi r}} f_{ij}(\theta)n_j, \tag{20}$$

where K_A is the stress intensity due to applied loads, n_j is the j component of the outward unit normal to bounding surface, (r,θ) are polar coordinates measured from the crack tip and f_{ij} is a given function that can be found in the work by Rice (1968).

For both the diffusion and elasticity problems the same finite element mesh is used. The finite element discretization divided the domain (see Fig. 1) into 18 equal angular zones and 100 geometrically scaled radial zones. Thus the mesh consisted of 1782 four-noded isoparametric equilateral rectangles and 18 four-noded isoparametric degenerate isosceles triangles, with a total of 1901 nodes. Geometric scaling of the radial lengths allowed for fine near tip discretization to ensure accurate modeling of the hydride zone with regard to both hydrogen diffusion and elasticity. The distance

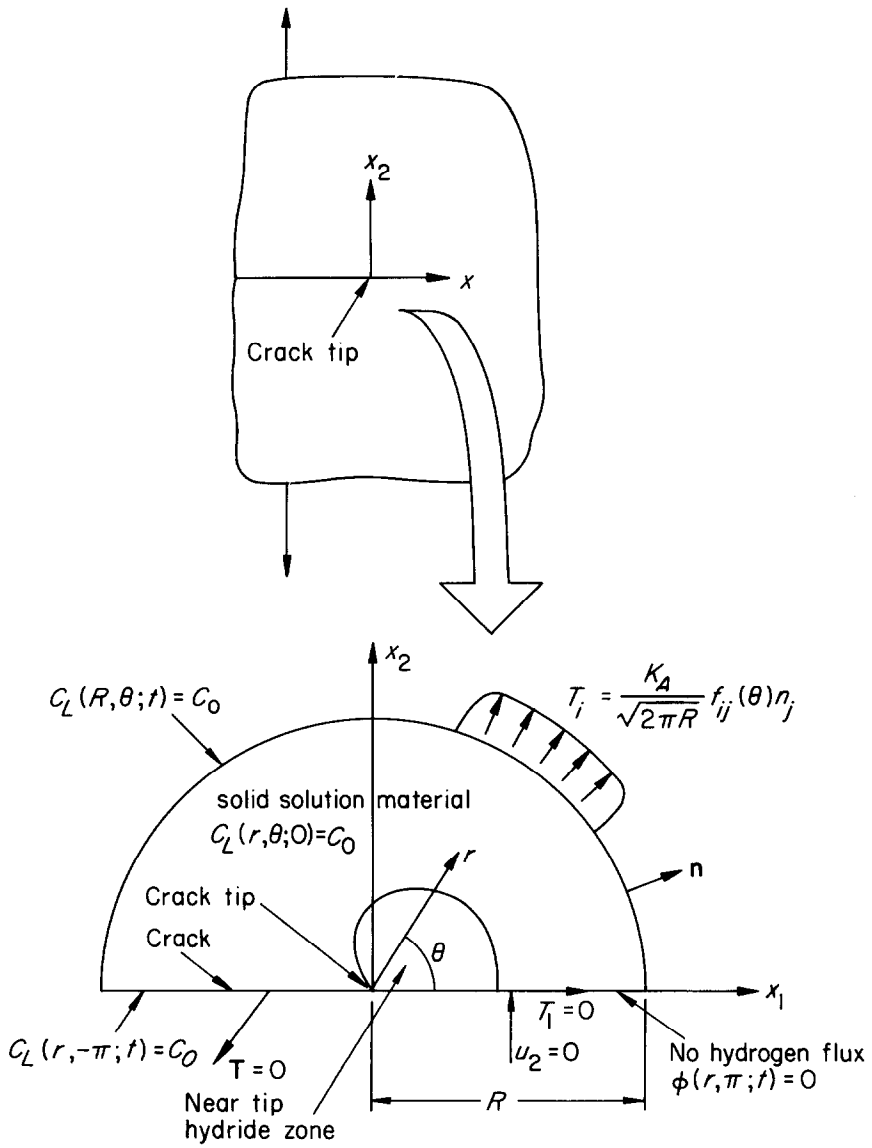

Fig. 1. The coupled initial boundary value diffusion problem and elastic boundary value problem of a semi-infinite crack with the hydride zone formed near the crack tip under mode I tensile opening load.

from the crack tip to the outer boundary was set to equal 10 cm, although about half of the elements were within 1 micron from the crack tip.

As an initial condition, the hydrogen is assumed to have already diffused into the stress-free solid and a uniform concentration $C_L = C_0$ exists throughout the volume. The initial concentration is chosen below the stress-free terminal solid solubility and therefore there is no hydride at time $t = 0$, hence initially $f = 0$ and $\dot{f} = 0$. Hydrogen enters the material through the crack surfaces and the outer boundary (see Fig. 1)

which are kept at fixed concentration $C_L = C_0$ at any time $t > 0$. These boundary conditions correspond to formation of the crack tip hydrides under conditions of constant chemical potential. The alternative condition of crack hydride formation under constant hydrogen concentration in the specimen would correspond to no hydrogen flux across the crack surfaces. The outer boundary would be at a fixed concentration, $C_L = C_0$ as it would be chosen at sufficient distance from the crack tip to avoid any hydrogen depletion effects caused by the hydride formation. The loads are incrementally applied in a linear fashion, increased to levels which encourage the formation of a zone of hydride large enough to be accurately monitored by the near tip elements and then held at a constant level. Geometric symmetry conditions are taken into account for both diffusion processes and the mechanics problem.

All material parameters were chosen to approximate the niobium–hydrogen system. The molar volume of niobium, V_M, equals 10.852×10^{-6} m^3/mol, the partial molar volume of hydrogen in solution with niobium, V_H, is estimated to be 1.888×10^{-6} m^3/mol (Peisl, 1978) and the molar volume of the hydride in the two-phase composite, V_{hr}, is equal to 12.3×10^{-6} m^3/mol (Hindin and Birnbaum, 1981). The terminal solid solubility of hydrogen in solution is given by (1) with $A = 3.74$ and $(H_h + W_{acc}) = -10.6$ kJ/mol (Puls, 1978; Hindin and Birnbaum, 1981; Sofronis, 1987). The system's temperature is taken to be 300 K, where at this temperature the terminal solid solubility of hydrogen in solution at zero stress is $c_s^0 = 0.054$ hydrogen atoms per solution atom by (1). The activation energy for hydrogen diffusion through hydride was taken equal to three times the activation energy for diffusion through the solid solution phase. Thus at 300 K the diffusion constant of solute hydrogen through the metal, D_s, is equal to 8.3×10^{-10} m^2/s (Völkl and Alefeld, 1978) and the diffusion constant of hydrogen through the hydride, D_h, is equal to 2.3×10^{-13} m^2/s. Young's modulus of the material is 113.65 GPa, Poisson's ratio is 0.39, $\theta_{hr} = 0.12$, and $\theta_h = 0.174$. Plastic yielding is suppressed since the mechanical behavior is modeled as elastic.

A variational description of the hydrogen diffusion and hydride precipitation initial value problem can be obtained (Sofronis and McMeeking, 1989). By means of this variational statement, the finite element equations are derived (see Appendix). Numerical integration of the non-linear diffusion equation is carried out by a modified backward Euler method (Sofronis and McMeeking, 1989). The discretized finite element equations for the non-linear elastic boundary value problem are coupled to the diffusion equation. Solutions to the coupled equations are obtained via a numerical scheme based on the forward Euler method and implemented with small increments of load and time (see Appendix). The stiffness derivative method (Parks, 1974, 1977) was used to determine the local stress intensity factor at the crack tip.

4. NUMERICAL RESULTS

Numerical calculations were carried out while the system's initial concentration c_0, measured in hydrogen atoms per solution atom was less than the stress-free terminal solid solubility limit c_s^0. At time $t = 0$ a mode I opening load was applied and its magnitude was increased linearly with time to a maximum value reached at time t_l.

At all other times greater than the loading time t_l the load was held fixed at the maximum level.

First the development of the hydride zone in time was studied using a nominal hydrogen concentration of 0.001 H/M (H/M denotes hydrogen atoms per metal atom) and a loading time of $t_l = 10^{-4}$ s at which the maximum load corresponded to an applied stress intensity factor $K_A = 10$ MPa$\sqrt{m}$. Surface plots of the hydride volume fraction around the crack tip at the origin for times of $t = 10^{-4}$, 10^{-3}, 10^{-2}, 0.1, 1, 100 s under fixed load, $K_A = 10$ MPa$\sqrt{m}$, clearly show that hydride formation occurs initially at the crack tip (Fig. 2). Figure 3 shows the respective contours of hydride volume fraction $f = 0.5$. The same figure shows the theoretical isobars $\sigma_{kk}/3E = 0.077$ and 0.047 for the unperturbed crack tip field at $K_A = 10$ MPa$\sqrt{m}$ which coincide with the hydride curves $f = 0.5$ at times $t = 10^{-4}$, 10^{-3} s on the x_2 axis (Fig. 1). Figures 2 and 3 confirm the existence of a hydride zone in front of the crack tip during loading, as the loading is just completed at time $t = t_l = 10^{-4}$ s. While the loading is abrupt, there is still time enough for some hydride to form near the crack tip during the loading process. Also evident from Fig. 2(e) and (f) is the apparent lack of growth in

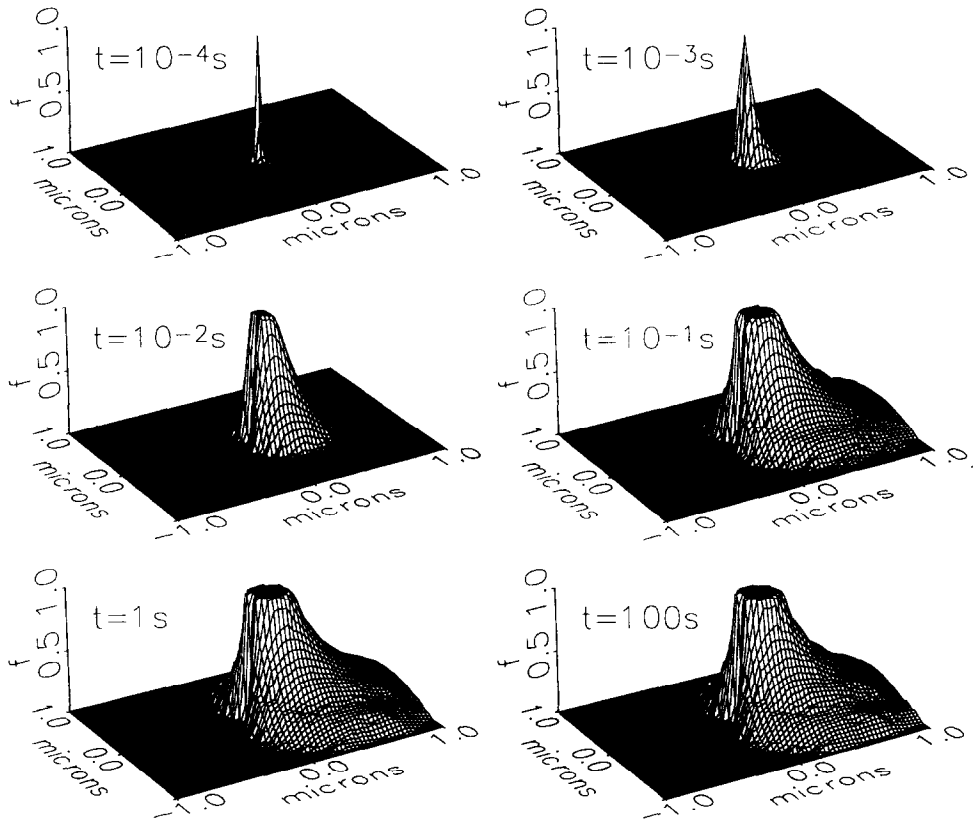

Fig. 2. Surface plots of the hydride volume fraction, f, around a crack tip at a fixed load of $K_A = 10$ MPa$\sqrt{m}$ which was applied in 10^{-4} s. The initial hydrogen concentration equals 10^{-3} H/M.

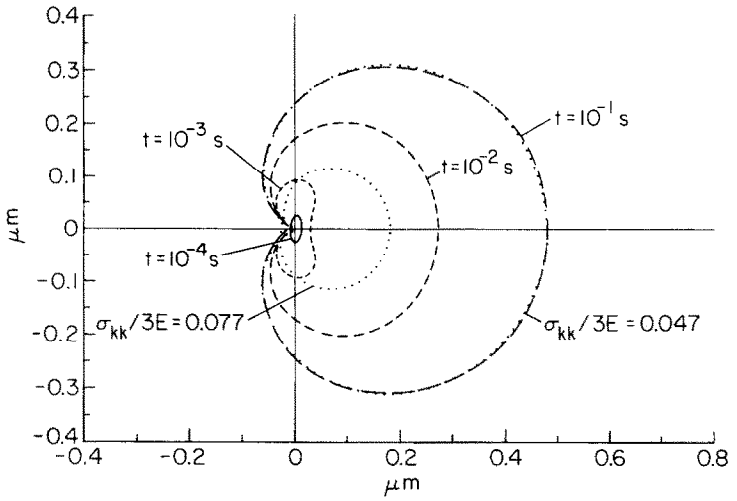

Fig. 3. Contour of the hydride volume fraction, $f = 0.5$, around a crack tip at a fixed load of $K_A = 10$ MPa$\sqrt{m}$ applied in 10^{-4} s plotted. Also shown are the theoretical isobars $\sigma_{kk}/3E = 0.077$, 0.047 from the unperturbed solution. The initial hydrogen concentration equals 10^{-3} H/M.

the hydride zone after time approximately equal to 1 s, an indication that the equilibrium state of hydride formation with the local stress has been approached. Figure 3 shows that at the early times of hydride formation, $t = 10^{-4}$, 10^{-3} s, the shape of the contours $f = 0.5$ differs from that of the isobar $\sigma_{kk}/3E = 0.077$. However, once the equilibrium has been reached, namely after $t = 0.1$ s, the corresponding curve $f = 0.5$ and the isobar $\sigma_{kk}/3E = 0.047$ coincide. The deviation of the hydride contours from the isobars at the early times results from the hydrogen flux across the crack surfaces which dominates over volume diffusion at early times.

The dependence of the time necessary for the hydride formation to reach equilibrium conditions on the loading time, t_l, was investigated by carrying out additional calculations with $t_l = 10^{-2}$ and 1 s. The corresponding equilibrium solutions at time $t = 100$ s are identical for all cases, $t_l = 10^{-4}$, 10^{-2} and 1 s, which indicates that the equilibrium solution corresponding to a given applied load is insensitive to the rate at which the load is reached, as expected. However, since the local crack tip stress intensity factor is affected by the near tip hydride precipitation (to be discussed shortly) and this does depend on t_l during the time prior to equilibrium, the local crack tip stress intensity at short times depends strongly on the loading time rate prior to achieving equilibrium.

Figure 4 shows the hydride volume fraction ahead of the crack tip at $\theta = 0$ plotted against normalized distance $r/(K_A/E)^2$ from the crack tip at two different load levels of $K_A = 2$ and 10 MPa$\sqrt{m}$, time $t = 100$ s, initial hydrogen concentration of 0.001 H/M and loading time of $t_l = 10^{-4}$ s. Clearly the size of the fully developed equilibrium hydride zone scales directly with the level of the applied load for the given fixed initial hydrogen concentration. The dependence of the equilibrium zone size on the initial hydrogen concentration is shown in Fig. 5 where the hydride volume fraction ahead of the crack tip at $\theta = 0$ is plotted against normalized distance $r/(K_A/E)^2$ from the

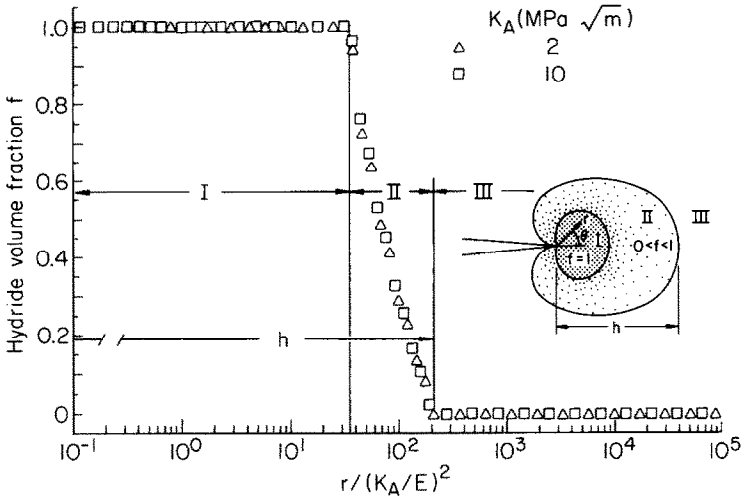

Fig. 4. Plot of the hydride volume fraction, f, versus normalized distance $r/(K_A/E)^2$ ahead of the crack tip at $\theta = 0$ after 100 s when hydride formation reached equilibrium with local stress due to applied loads of $K_A = 2$ and 10 MPa$\sqrt{m}$ and an initial hydrogen concentration of 10^{-3} H/M.

crack tip at time $t = 100$ s for initial concentrations of 10^{-4}, 10^{-3}, 10^{-2} H/M. Figure 6 shows the local hydrogen concentration, c_s, and the terminal solid solubility of hydrogen, c_s^σ, ahead of the crack tip at $\theta = 0$ plotted against normalized distance $r/(K_A/E)^2$ from the crack tip at time $t = 100$ s at equilibrium under load levels of $K_A = 2$ and 10 MPa$\sqrt{m}$ and an initial hydrogen concentration of 0.001 H/M. The solute hydrogen concentration from the crack tip to $r/(K_A/E)^2 = 10$ is zero as that region is fully hydrided, $f = 1$. For the normalized distance $10 < r/(K_A/E)^2 < 37$,

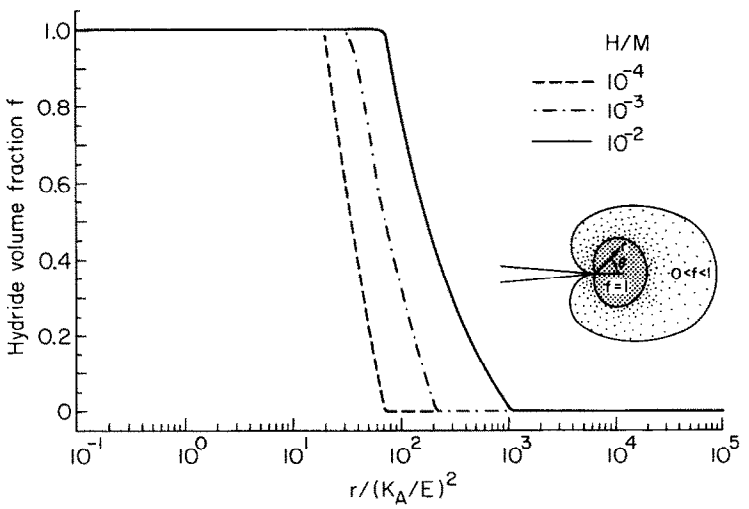

Fig. 5. Plot of the hydride volume fraction, f, in equilibrium with local stress versus normalized distance $r/(K_A/E)^2$ ahead of the crack tip at $\theta = 0$ at various initial concentrations of hydrogen, H/M.

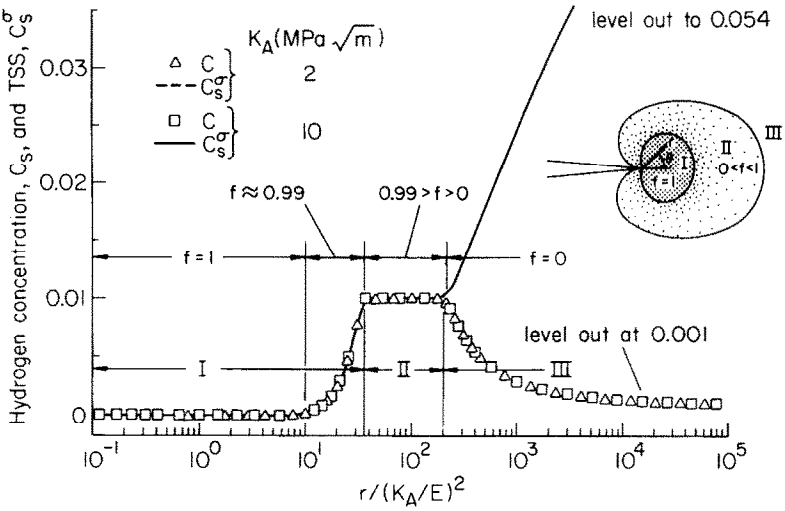

Fig. 6. Plot of the hydrogen concentration c_s, in atoms per solution atom, and terminal solid solubility c_s^σ versus normalized distance $r/(K_A/E)^2$ ahead of the crack tip at $\theta = 0$ when hydride formation has reached equilibrium with local stress at an initial hydrogen concentration of 10^{-3} H/M.

$0.99 < f < 1$ and the solute hydrogen concentration, c_s increases from 0 to the value in equilibrium with the hydride in front of the crack tip, $c_s = c_s^\sigma \approx 0.01$. At distances of $37 < r/(K_A/E)^2 < 200$, $0 < f < 0.99$ and the solute concentration remains at $c_s^\sigma \approx 0.01$. At distances greater than $r/(K_A/E)^2 = 200$ there is no stress induced hydride and the solute concentration decreases to the initial concentration of H/M = 0.001 while the solvus concentration increases toward the value of the stress-free solvus, H/M = 0.054. At all distances the local concentrations of hydrogen and the stress dependent terminal solid solubility scale with the applied loads.

Figures 4 and 6 are consistent with hydride formation occurring initially in the immediate vicinity of crack tip because the hydrostatic stress attains its maximum value there in the elastic stress solution at any load level, thereby causing maximum reduction of the local TSS. Under the same conditions, Fig. 7 shows the dimensionless hydrostatic stress $\sigma_{kk}/3E$ ahead of the crack tip at $\theta = 0$ as it scales with normalized distance $r/(K_A/E)^2$ from the crack tip. For the purposes of comparison, the results of a hydrogen-free case are also included in Fig. 7. In the absence of hydrogen, the stress solution for the crack tip region is the singular crack tip stresses for mode I opening of the crack. Since the dilatations induced by the hydride forming in the vicinity of the crack tip and the local hydrogen in solution are constrained by the surrounding material, self stresses develop in and near the hydride zone. These stresses change the magnitude of the singular components at the crack tip so that the local elasticity solution is characterized by $K_t = K_A + \Delta K$ where ΔK is a shielding or antishielding contribution (depending on its sign) to the stress intensity factor, K_A, which arises due to the hydride formed and the hydrogen in solution near the crack tip (McMeeking and Evans, 1982; Lufrano and Sofronis, 1995). In Fig. 8 stress intensity factors K_A and K_t are plotted versus time t when the nominal hydrogen concentration is H/M = 10^{-3}, the loading time is $t_l = 5 \times 10^{-4}$ s and the final maximum applied load

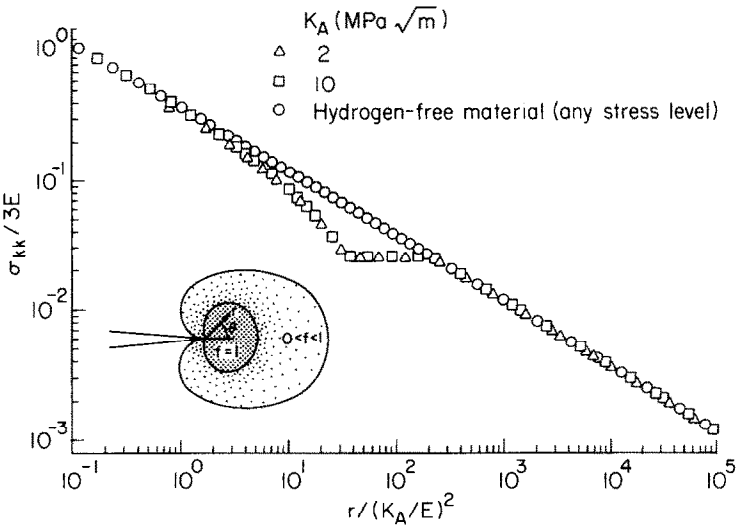

Fig. 7. Plot of normalized hydrostatic stress $\sigma_{kk}/3E$ versus normalized distance $r/(K_A/E)^2$ ahead of the crack tip at $\theta = 0$ when hydride formation has reached equilibrium with local stress due to applied loads of $K_A = 2$ and 10 MPa$\sqrt{m}$ at an initial hydrogen concentration of 10^{-3} H/M.

corresponds to a $K_A = 10$ MPa$\sqrt{m}$. During the transient stage of hydrogen diffusion, the parameter K_t is less than K_A; at the time the maximum load is reached, $t = t_l$, the calculated stress intensity factor at the crack tip, K_t, is as much as 10% lower than K_A. However, as the time elapses and the system progresses toward equilibrium with the applied load, K_t becomes equal to K_A; a consequence of the purely dilatant character of the distortion field for the hydride and for solute hydrogen (McMeeking

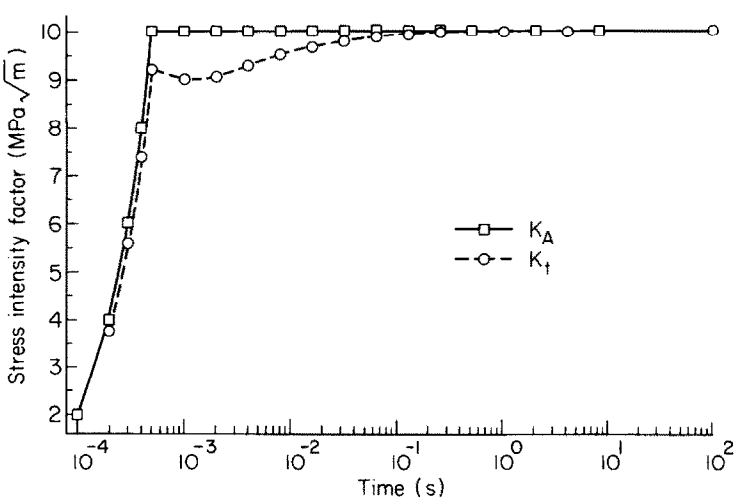

Fig. 8. Plot of applied stress intensity factor, K_A, and local crack tip stress intensity factor, K_t, versus time, t, under maximum applied load of $K_A = 10$ MPa$\sqrt{m}$, loading time $t_l = 5 \times 10^{-4}$ s and initial hydrogen concentration of 10^{-3} H/M.

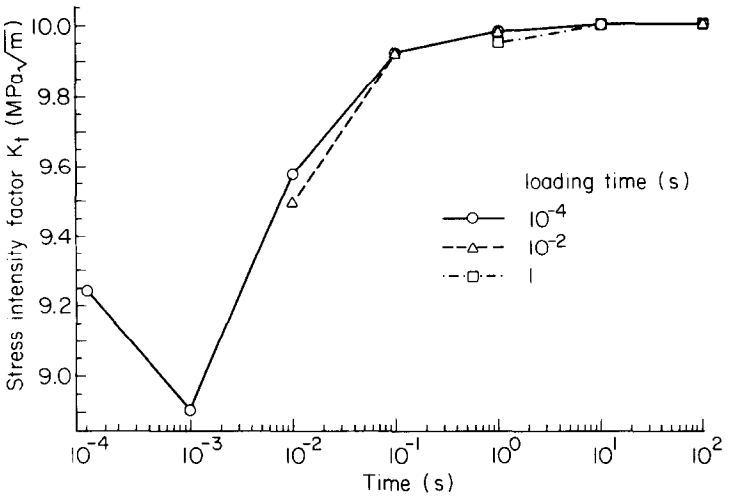

Fig. 9. Plot of local crack tip stress intensity factor K_t versus time t, under maximum applied load of $K_A = 10$ MPa$\sqrt{m}$, loading times of 10^{-4}, 10^{-2} and 1 s and initial hydrogen concentration of 10^{-3} H/M.

and Evans, 1982). The purely dilatational nature of the distortion field of the solute hydrogen is in agreement with experiments (Peisl, 1978). The distortion field due to the hydride should have shear components (relatively small in magnitude) since the hydride generally differs in crystal symmetry from the solid solution.

Figure 9 shows the strong effect of the loading rate on the transient behavior of the crack tip stress intensity factor, K_t. The effect is investigated for three loading times, $t_l = 10^{-4}$, 10^{-2}, 1 s, final maximum applied load of $K_A = 10$ MPa$\sqrt{m}$, and initial hydrogen concentration, H/M, of 10^{-3}. When equilibrium is reached, $K_t = K_A$ and this is independent of the loading time, t_l. When the loading is abrupt, $t_l = 10^{-4}$ s, the loading is "ahead" of the diffusion and hydride formation and crack tip shielding is evident until the equilibrium state is reached at which $K_t = K_A$. In the initial times of this diffusion "limited" case, the hydrogen flux to the crack tip is dominated by short range diffusion of hydrogen through the free surfaces of the crack (maintained at the initial concentration) and the local hydrostatic stress gradients close to the surfaces of the crack are greater than those immediately ahead of the crack tip. As a result, precipitates form initially more rapidly in the region outside the 120° fan ($-\pi/3 < \theta < \pi/3$) ahead of the tip as the concentration of hydrogen on the crack surfaces is always maintained at the nominal level. This is demonstrated by the contour plots of Fig. 3 which show that at the early times of hydride formation the constant hydride fraction contours are not similar to the isobars, with more hydride forming at the sides of the crack than in front of the crack tip. Precipitation within the $-\pi/3 < \theta < \pi/3$ fan can only be continued with long range diffusion of hydrogen from sites further afield. The dominance of hydride formation outside of $-\pi/3 < \theta < \pi/3$ in the early stages of hydride formation results in crack tip shielding, $\Delta K < 0$ (McMeeking and Evans, 1982). This crack tip shielding disappears as equilibrium is attained, $K_t \rightarrow K_A$, and the $f = 0.5$ contour is identical to the isobar (Fig. 3). When the loading is slow, e.g. $t_l = 1$ s, (Fig. 9), hydrogen diffusion is sufficiently high

to allow the hydride distribution to approximate the equilibrium distribution at all times. As a result there is little crack tip shielding induced by the near equilibrium hydride formation (McMeeking and Evans, 1982). These non-equilibrium, transient crack shielding effects are not expected to be present for calculations carried out under conditions where there is no hydrogen transfer across the crack surfaces.

5. DISCUSSION

In the calculations, hydride precipitation has been induced in a system with an initial uniform hydrogen concentration well below the stress-free solvus. Hydrostatic stress gradients generated solvus gradients and, in turn, hydrogen flux was established. It is to be emphasized that this flux is in addition to that which results from the hydrostatic stress drift effect. The results shown in Figs 4 and 5 suggest that when hydride formation reaches equilibrium with local stresses, the shape of the hydride zone is self-similar, namely it scales directly with the applied load. At this stage the contours of the equal volume fraction of hydride have the shape of the contours of the constant hydrostatic stress (Fig. 3). In addition, it was found that the shape of the equilibrium solution is independent of the rate at which the load is applied. At any given initial concentration of hydrogen, the equilibrium situation ahead of the crack tip is characterized by:

(a) A fully hydrided ($f = 1$) near tip inner zone I directly ahead of the crack tip (Figs 4–6), and a local stress field which is unperturbed by the presence of the hydride, $K_t = K_A$ (Figs 7–9). The zero effect on the K_A results from the dominance of the hydride formation by the local hydrostatic stress (McMeeking and Evans, 1982).

(b) A transition middle zone II that is much broader than the inner zone ahead of the crack tip, in which the hydride volume fraction f diminishes rapidly with distance from the tip (Figs 4 and 5), the local hydrogen concentration equals the local solvus (Fig. 6) and the stresses are constant (Fig. 7). At the border between the inner and middle zone the TSS of hydrogen rises very rapidly from a very small value to reach a constant level in accordance with the constant hydrostatic stress level.

(c) An outer zone III consisting of solid solution alone, $f = 0$, (Figs 4 and 5) where the terminal solid solubility of hydrogen is greater than the local hydrogen concentration (Fig. 6) and increases to the stress-free value. The local hydrogen concentration decays from its plateau level in the transition zone to the nominal stress-free levels prevailing at the outer boundary of the domain. The stress field within this outer zone is the same as that obtained for the elastic solution in the absence of hydrogen and is characterized by K_A (Figs 7–9).

The size of the equilibrium hydride zone, h, ahead of the crack tip can be estimated from the equilibrium solution to (8) in the absence of hydride via

$$C_L = C_0 \exp\left(\frac{\sigma_{kk} V_H}{3RT}\right), \tag{21}$$

where

$$\sigma_{kk} = \frac{2(1+v)K_A}{\sqrt{2\pi r}} \cos\left(\frac{\theta}{2}\right), \tag{22}$$

C_L is the local hydrogen concentration in the lattice, and C_0 is the initial concentration of hydrogen (both expressed as hydrogen atoms per unit volume of solid solution). At equilibrium, the perimeter of the hydride zone is determined by setting $C_L = C_{LS}$, where C_L is given by (21), C_{LS} is defined through (11) in which $c_s = c_s^\sigma$ with the solvus c_s^σ computed from (1), and use of (6) with $a = c_s^\sigma/(1-c_s^\sigma)$ is made. This leads to

$$\ln\left[\frac{c_s^\sigma}{(1-c_s^\sigma)c_0}\right] + \frac{V_H\left(\frac{1-2c_s^\sigma}{1-c_s^\sigma}\right)\ln\left(\frac{c_s^\sigma}{c_s^0}\right)}{V_{hr} - \left(V_M + \frac{V_H c_s^\sigma}{1-c_s^\sigma}\right)} = 0 \tag{23}$$

for the calculation of the solvus c_s^σ at the boundary of the hydride zone, $f = 0$, and to

$$\frac{h}{\left(\frac{K_A}{E}\right)^2} = \frac{2(1+v)^2}{9\pi}\left[\frac{\frac{EV_H}{RT}}{\ln\left(\frac{c_s^\sigma(1-c_0)}{(1-c_s^\sigma)c_0}\right)}\right]^2 \tag{24}$$

for the calculation of the distance h of the crack tip to the hydride zone perimeter at $\theta = 0$, where c_s^0 is the stress-free solvus, and c_0 is the initial concentration expressed as hydrogen atoms per solution atom. Equation (23) is plotted in Fig. 10 in which

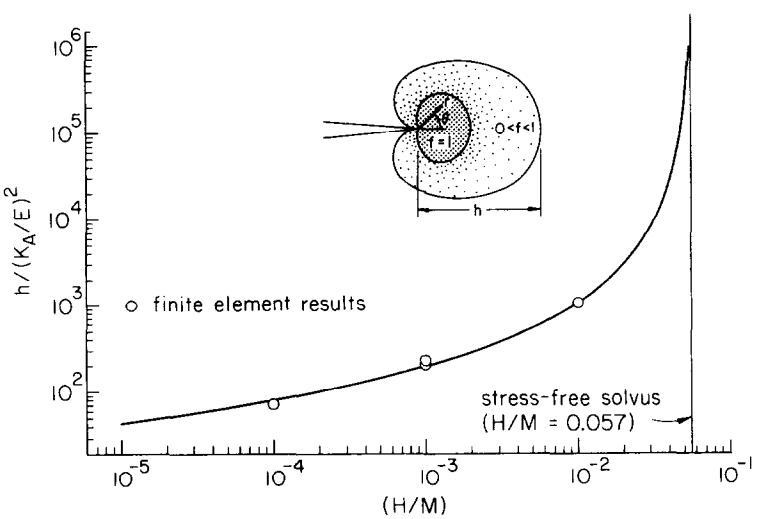

Fig. 10. Plot of normalized hydride zone size, $h/(K_A/E)^2$, directly ahead of the crack tip at $\theta = 0$ versus initial hydrogen concentration, H/M. The stress-free terminal solid solubility of hydrogen equals 0.057 H/M at temperature 300 K.

the normalized hydride zone size, $h/(K_A/E)^2$, is shown as a function of the initial concentration of hydrogen, H/M. As the initial concentration approaches the stress-free solvus the hydride zone size becomes unbounded. In the same figure the finite element results (Fig. 5) for nominal concentration 10^{-4}, 10^{-3}, 10^{-2} H/M are also shown as points. Since the finite element prediction of $h/(K_A/E)^2$ is identical to the analytical prediction of (24), one can directly use (24) or Fig. 10 to calculate the equilibrium hydride zone size for given applied stress intensity factor and initial concentration of hydrogen.

While the chosen boundary conditions apply for the case of constant hydrogen chemical potential, e.g. a gaseous hydrogen atmosphere with hydrogen transfer across the crack faces, the equilibrium results are equally applicable for the case of hydride precipitation in a system where the hydrogen is supplied by internal solute hydrogen. The only significant difference is observed during the initial period of transient precipitation where crack tip shielding is observed due to the deviation of the constant hydride contours from the equilibrium contours. These deviations result from the flux of hydrogen into the solid across the crack tip flanks; an effect which is not present in the case of hydride precipitation from solute hydrogen alone. In the case of hydride formation from gaseous hydrogen (constant chemical potential), crack tip shielding occurs during the initial diffusion transient and it increases with the loading rate and decreases with time as the equilibrium distribution where $K_t = K_A$ is attained.

Due to the absence of any antishielding effects during hydride formation, no crack growth is expected if the hydride forms under an applied stress intensity factor $K_A < K_{IC}^h$, where K_{IC}^h is the fracture toughness of the brittle hydride (Gahr *et al.*, 1977, 1980). As the hydrides are extremely brittle, with fracture toughness of the order of 1 MPa$\sqrt{m}$ (Gahr *et al.*, 1980; Simpson and Puls, 1979), any stress intensity factor, K_A, above this low value of K_{IC}^h will tend to cause crack propagation once a hydride zone has formed. This crack propagation process will be stable since the crack will grow toward tougher material with less hydride. In addition, as the crack grows, a wake of hydride will be left behind provided that the hydride does not dissolve upon unloading (e.g. for hydrides exhibiting some plastic accommodation). The dilated hydride zone in the crack wake will generate constraint stresses which will tend to reduce the crack tip stress intensity factor, $\Delta K < 0$, (McMeeking and Evans, 1982). This clamping effect has been observed by Shih *et al.* (1988) in titanium and may be sufficiently strong to deter the crack from further growth unless K_A is increased. The process of crack growth may be repeated by the new hydride precipitation that will occur at the tip combined with an appropriate increase of the applied stress intensity factor.

The methodology of McMeeking and Evans (1982) and Budiansky *et al.* (1983) may be used to estimate the clamping effect of the hydride zone in the wake of an advancing crack tip and to calculate the threshold stress intensity factor for continued crack growth. The relevant result is for a material with a transformation zone in which the contours of equal phase change dilatancy are the isobars ahead of the crack tip and there is a wake parallel to the crack behind the tip (Fig. 11). This gives

$$\Delta K = \frac{E}{6\sqrt{2\pi}(1-v)} \int_A f r^{-3/2} \cos\left(\frac{3\theta}{2}\right) \mathrm{d}A, \tag{25}$$

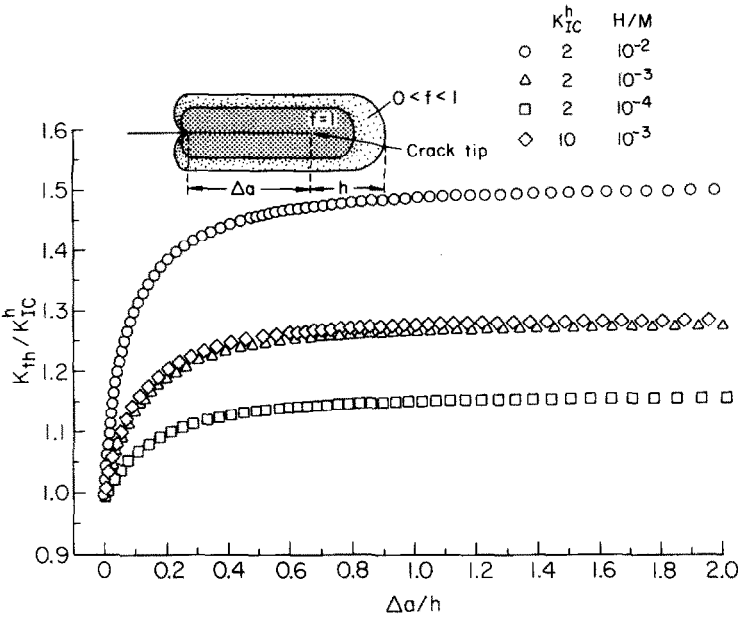

Fig. 11. Plot of normalized threshold stress intensity factor, K_{th}/K^h_{IC}, for steady state crack growth versus normalized crack advance, $\Delta a/h$, at various initial concentrations of hydrogen, H/M, and hydride fracture toughness $K^h_{IC} = 2, 10$ MPa$\sqrt{m}$.

where A is the transformation zone area and r, θ are polar coordinates at the crack tip. In calculating the integral of (25) the finite element results shown in Figs 2(e) and 5 for the distribution of f in the equilibrium hydride zone were used. Crack growth occurs when $K_t = K^h_{IC}$ which in conjunction with equations $K_t = K_A + \Delta K$ and (25) gives the threshold applied stress intensity factor, $K_{th} = K^h_{IC} - \Delta K$, for continual growth. In Fig. 11 the normalized threshold stress intensity factor, K_{th}/K^h_{IC}, is shown plotted versus normalized crack advance, $\Delta a/h$, at various initial hydrogen concentrations, H/M. Clearly Fig. 11 shows an R-curve behavior which is independent of the fracture toughness of the hydride and strongly dependent on the initial hydrogen concentration. The former property is due to the scaling of the hydride zone size, h, with the applied stress intensity factor and the latter is due to the dependence of h upon the initial hydrogen concentration. As the crack advances K_{th} rises, and after a normalized crack advance of $\Delta a/h \approx 1, 0.6, 0.3$, respectively, for initial concentrations of 10^{-4}, 10^{-3}, 10^{-2} H/M it reaches 95% of its asymptotic value which strongly depends upon the initial concentration. Thus for an initial concentration of hydrogen of 0.01 H/M the asymptotic threshold stress intensity factor is about 50% higher than the fracture toughness of the hydride. It should be noted that in the calculations of McMeeking and Evans (1982) the asymptotic threshold stress intensity factor is attained when the crack advance exceeds the zone width by ~ 5. This corresponds to a normalized crack advance $\Delta a/h$ equal to 3.75. However, the McMeeking and Evans (1982) calculations correspond to fully transformed zones whereas the calculations of the present paper involve a partially hydrided zone surrounding the fully hydrided one around the crack. The ratio of the size of the hydride zone, h, to the distance

directly ahead of the tip of the most remote contour $f = 1$ can be inferred from Fig. 5 to be 3.5, 6.56, 15.31 for initial concentrations 10^{-4}, 10^{-3}, 10^{-2} H/M. Therefore if one linearly extrapolates the McMeeking and Evans result to treat the additional effect of the partially transformed zones, the crack advance required for asymptotic toughness in the case of the calculations of the present paper would be 3.75/3.5, 3.75/6.56, 3.75/15.31, respectively, for initial concentrations of 10^{-4}, 10^{-3}, 10^{-2} H/M. Hence the extrapolated predictions of the McMeeking and Evans model agree closely with the numerical results of the present work.

Thus, a threshold toughness for continual crack growth above the fracture toughness of the pure hydride can be predicted when there is no plasticity in the matrix. Such thresholds have been observed in zirconium (Simpson and Puls, 1979) and titanium (Shih *et al.*, 1988) although limited yielding did occur in these cases. Assessing the fracture behavior of the material one can use the present results as follows. First the information of Fig. 11 allows one to predict whether for a given nominal concentration of hydrogen and applied stress intensity factor a crack will run through the hydride zone unopposed by the clamping effect of the wake leading eventually to brittle fracture. If the applied stress intensity factor is less than the asymptotic threshold toughness and hence brittle fracture does not occur, then with use of (24) the hydride zone size, h, for the given initial concentration is predicted and from Fig. 11 the amount of critical crack advance before brittle fracture can be estimated.

The foregoing calculations are based on a purely dilatational transformation strain at the hydrides. It is known, however, that the transformation strain is anisotropic (Somenkov *et al.*, 1968; Rashid and Scott, 1973; Schober, 1975; Pick and Bausch, 1976) and hence the hydride formation should respond to the deviatoric components of the crack tip stress field as well as to the dilatational components. Numerically however, the largest stress contributions to the hydride free energies arise from the dilatational components.

The calculations yield a point density of the hydrides and do not address the issues associated with hydride shapes. For systems which accommodate the hydride volume change by elastic strain, the hydrides tend to form in a plate morphology along specific crystallographic planes, which minimizes the elastic energy of the system (Takano and Suzuki, 1974). In contrast, systems in which the volume change is partially accommodated by plastic deformation of the matrix tend to form "blocky hydrides" which can have dendritic morphologies (Grossbeck and Birnbaum, 1977). While the hydride morphology does not affect the main result of these calculations, it does affect the details of the crack propagation through the hydrides once $K_A > K_{th}$.

Accommodation of the volume change which accompanies the hydride formation by plastic deformation of the matrix has several additional effects on the crack tip behavior. In addition to the effects on the hydride morphology, partial accommodation by matrix plasticity relaxes the elastic constraints on the hydrides which lead to crack tip clamping and hence makes it easier for the crack to propagate through the hydride.

Additionally, some of the dilation which accompanies the hydride formation will be accomodated by plastic flow thereby lessening the interaction between the crack tip dilatational stresses and the volume changes accompanying the hydride precipitation. A system which exhibits plasticity at the crack tip also has a smaller local

stress field as a result. Both of these effects have the consequence that the hydride zone at the crack tip will be smaller than in the purely elastic case.

While plasticity accompanying the hydride formation at the crack tip has consequences for some of the detailed hydride precipitation and cracking behavior, the general effects which are calculated in the purely elastic case remain and the elastic behavior is a good approximation, even in the case of limited plasticity. This is particularly true at distances from the crack tip of less than about two crack opening displacements where both the hydrostatic stress and the hydrogen concentration would achieve the maximum values. Precipitation in the case of limited plasticity would still occur predominantly inside the 120° fan and the net effect is no crack tip shielding. The plasticity effect requires a more careful treatment of the effects of local plasticity and this will be carried out in a subsequent publication.

The present calculation treats the kinetics of hydride precipitation at a stationary crack. Calculations at propagating cracks will be carried out to examine the dynamics of crack propagation in hydrogen embrittlement accompanied by hydride formation. For the case of a propagating crack, the kinetics will be very strongly affected by the nature of the hydride accommodation. In the case of elastic accommodation, the hydrides behind the crack tip will redissolve (Takano and Suzuki, 1974) and serve as a source of solute hydrogen for further precipitation in front of the crack tip. This can lead to a steady state crack propagation rate. Plastic accommodation of the hydride serves to stabilize the hydrides against resolution (Birnbaum *et al.*, 1976) and hence the hydrogen must diffuse to the crack tip from increasing distances as cracking occurs, leading to a decreasing crack propagation rate.

6. CLOSURE

An example of hydride formation at a stationary crack tip under external stress in niobium has been presented. The model assumes elastic accommodation of the hydrides and is based on a purely dilatant transformation strain upon precipitation. Under fixed temperature and nominal concentration of hydrogen the equilibrium hydride zone size scales with the applied loads. A threshold for continual crack growth has been predicted and this threshold is above the fracture toughness of pure hydride and depends on the nominal concentration of hydrogen away from the tip.

ACKNOWLEDGEMENT

This work was supported by the Department of Energy under grant DEFGO2-91ER45439.

REFERENCES

Birnbaum, H. K. (1979) Hydrogen related failure mechanisms in metals. *Environmental Sensitive Fracture of Engineering Materials* (Proceedings of Symposium on Environmental

Effects on Fracture, Chicago, Illinois, 24–26 October, 1977) (ed. Z. A. Foroulis), pp. 326–360. Metallurgical Society of AIME, Warendale, PA.

Birnbaum, H. K. (1983) Hydrogen related fracture of metals. *Atomistics of Fracture* (Proceedings of a NATO Advanced Research Institute on Atomistics of Fracture, Calcatoggio, Corsica, France, 22–31 May, 1981) (ed. R. M. Latanision and J. R. Pickens), pp. 733–765. Plenum Press, NY.

Birnbaum, H. K. (1984) Hydrogen related second phase embrittlement of solids. *Hydrogen Embrittlement and Stress Corrosion Cracking* (Proceedings of a Troiano Festchrift Symposium, Case Western Reserve University, 1–3 June, 1980) (ed. by R. Gibala and R. F. Hehemann), pp. 153–177. ASM, OH.

Birnbaum, H. K. and Sofronis, P. (1994) Hydrogen-enhanced localized plasticity—a mechanism for hydrogen-related fracture. *Mater. Sci. Engng* **A176,** 191–202.

Birnbaum, H. K., Grossbeck, M. L. and Amano, M. (1976) Hydride precipitation in Nb and some properties of NbH. *J. Less Comm. Met.* **49,** 357–370.

Budiansky, B., Hutchinson, J. W. and Lambropoulos, J. C. (1983) Continuum theory of dilatant transformation toughening in ceramics. *Int. J. Solids Struct.* **19,** 337 355.

Dutton, R. and Puls, M. P. (1976) A theoretical model for hydrogen induced subcritical crack growth. *Effect of Hydrogen Behavior of Materials* (ed. by A. W. Thompson and I. M. Bernstein), pp. 516–525. Metallurgical Society of AIME, NY.

Dutton, R., Nuttall, K., Puls, M. P. and Simpson, L. A. (1977) Mechanisms of hydrogen induced delayed cracking in hydride forming materials. *Met Trans.* **8A,** 1553–1562.

Dutton, R., Woo, C. H., Nuttall, K., Simpson, L. A. and Puls, M. P. (1978) The mechanism of hydrogen induced delayed cracking in zirconium alloys. *Hydrogen in Metals* (Proceedings of the 2nd International Congress, Paris, France, 6–10 June, 1977), Vol. 1, pp. 3C6 1–8. Pergamon Press, NY.

Ellyin, F. and Wu, J. (1994) Effect of hydride precipitation on the elastoplastic stress field near a crack tip. *Acta Metall.* **42,** 2709–2717.

Eshelby, J. D. (1956) The continuum theory of lattice defects. *Solid State Physics* (ed. F. Seitz and D. Turnbull), Vol. 3, pp. 79–144. Academic Press, NY.

Eshelby, J. D. (1957) The determination of the elastic field of an ellipsoidal inclusion and related problems. *Proc. R. Soc.* **A241,** 376–396.

Flannagan, T. B., Mason, N. B. and Birnbaum, H. K. (1981) The effect of stress on hydride precipitation. *Scr. Met.* **15,** 109–112.

Frankel, G. S. and Latanision, R. M. (1986) Hydrogen transport during deformation in nickel: Part I polycrystalline nickel. *Met. Trans.* **17A,** 861–867.

Gahr, S. and Birnbaum, H. K. (1978) Hydrogen embrittlement of Nb III—High temperature behavior. *Acta Metall.* **26,** 1781–1788.

Gahr, S., Grossbeck, M. L. and Birnbaum, H. K. (1977) Hydrogen embrittlement of Nb I—Macroscopic behavior at low temperatures. *Acta Metall.* **25,** 125–134.

Gahr, S., Makenas, B. J. and Birnbaum, H. K. (1980) Fracture of niobium hydrides. *Acta Metall.* **28,** 1207–1213.

Grossbeck, M. L. and Birnbaum, H. K. (1977) Low temperature hydrogen embrittlement of niobium II—Microscopic observations. *Acta Metall.* **25,** 135–147.

Hindin, B. S. and Birnbaum, H. K. (1981) Fracture kinetics of hydrogen embrittled niobium. Technical Report—Office of Naval Research (USN 00014-75-C-1012), University of Illinois at Urbana-Champaign, IL.

Hirth, J. P. (1987) Hydrogen induced fracture. *Chemistry and Physics of Fracture* (Proceedings of the NATO Advanced Research Workshop on Chemistry and Physics of Fracture, Bad Reichenhall, FRG, 23 June–1 July, 1986) (ed. by R. M. Latanision and R. H. Jones), pp. 538–551. Martinus Nijhoff Publishers, The Netherlands.

Ladna, B. and Birnbaum, H. K. (1987) A study of hydrogen transport during plastic deformation. *Acta Metall.* **35,** 1775–1778.

Li, J. C. M., Oriani, R. A. and Darken, L. S. (1966) The thermodynamics of stressed solids. *Z. Physik Chem. Neue Folge* **49,** 271–291.

Lufrano, J. and Sofronis, P. (1995) Numerical analysis of the interaction of solute hydrogen atoms with the stress field of a crack. To appear in the *Int. J. Solids Structures.*

McMeeking, R. M. and Evans, A. G. (1982) Mechanics of transformation-toughening in brittle materials. *J. Am. Ceram. Soc.* **65,** 242–246.

Peisl, H. (1978) Lattice strains due to hydrogen in metals. *Hydrogen in Metals I, Topics in Applied Physics* (ed. G. Alefeld and J. Volkl), Vol. 28, pp. 53–74. Springer-Verlag, NY.

Parks, D. M. (1974) A stiffness derivative finite element technique for determination of crack tip stress intensity factors. *Int. J. Fracture Mech.* **10,** 487–502.

Parks, D. M. (1977) The virtual crack extension method for nonlinear material behavior. *Comput. Methods App. Mech. Engng* **12,** 353–364.

Pick, M. M. and Bausch, R. (1976) The determination of the force-dipole tensor of hydrogen in niobium. *J. Phys. F: Metal Phys.* **6,** 1751–1763.

Puls, M. P. (1978) Hydrogen induced delayed cracking: 1. Strain energy effects on hydrogen solubility. Atomic Energy of Canada Limited Report, AECL-6302, Pinawa, Manitoba.

Puls, M. P. (1981) The effects of misfit and external stresses on the terminal solid solubility in hydride-forming metals. *Acta Metall.* **29,** 1961 1968.

Puls, M. P. (1984) Elastic and plastic accommodation effects on metal-hydride solubility. *Acta Metall.* **32,** 1259–1269.

Rashid, M. S. and Scott, T. E. (1973) Crystal structure of niobium hydrides. *J. Less Comm. Met.* **30,** 399–403.

Rice, J. R. (1968) Mathematical analysis in the mechanics of fracture. *Fracture: An Advanced Treatise* (ed. H. Liebowitz), Vol. 2, pp. 191–311. Academic Press, NY.

Schober, T. (1975) The niobium–hydrogen system—an electron microscope study. *Phys. Stat. Sol.* (a) **30,** 107–116.

Shalabi, A. F. and Meneley, D. A. (1991) Modeling of delayed crack initiation, *J. Engng Mater. Technol.* **113,** 443–448.

Shi, S. Q., Liao, M. and Puls, M. P. (1994) Modeling of the time dependent hydride growth at crack tips in zirconium alloys. Atomic Energy of Canada Limited Report, CoG-I-94-276, Pinawa, Manitoba.

Shih, D. S., Robertson, I. M. and Birnbaum, H. K. (1988) Hydrogen embrittlement of α titanium: in situ TEM studies. *Acta Metall.* **36,** 111–124.

Simpson, L. A. and Puls, M. P. (1979) The effects of stress, temperature and hydrogen content on hydride-induced crack growth in Zr–2.5%Nb. *Met. Trans.* **104,** 1093–1105.

Somenkov, V. A., Gurskaya, A. V., Zemlyanov, M. G., Kost, M. E., Chernoplekov, N. A. and Chertkov, A. A. (1968) Neutron scattering study of structure and phase transitions in niobium hydrides and deuterides. *Soviet Physics—Solid State* **10,** 1076–1082.

Sofronis, P. (1987) Mechanics of hydrogen embrittlement. Ph.D. Thesis, University of Illinois at Urbana-Champaign, Urbana, IL.

Sofronis, P. and Birnbaum, H. K. (1995) Mechanics of the hydrogen-dislocation–impurity interactions: part I—increasing shear modulus. *J. Mech. Phys. Solids* **43,** 49–90.

Sofronis, P. and McMeeking, R. M. (1989) Numerical analysis of hydrogen transport near a blunting crack tip. *J. Mech. Phys. Solids* **37,** 317–350.

Takano, S. and Suzuki, T. (1974) An electron-optical study of β-hydride and hydrogen embrittlement of vanadium. *Acta Metall.* **22,** 265–274.

Tien, J. K., Nair, S. V. and Jensen, R. R. (1981) Dislocation sweeping of hydrogen and hydrogen embrittlement. *Hydrogen Effects in Metals* (ed. I. M. Bernstein and A. W. Thompson), pp. 37–56. Metallurgical Society of AIME, NY.

Völkl, J. and Alefeld, G. (1978) Diffusion of hydrogen in metals. *Hydrogen in Metals I, Topics in Applied Physics* (ed. G. Alefeld and J. Völkl), Vol. 28, pp. 53–74. Springer-Verlag, NY.

Westlake, D. G. (1969) A generalized model for hydrogen embrittlement. *Trans. ASM* **62,** 1000–1006.

White, A. J., Sawatzky, A. and Woo, C. H. (1985) A computer model for hydride-blister in zirconium alloys. Atomic Energy of Canada Limited Report, AECL-8386, Pinawa, Manitoba.

APPENDIX: THE FINITE ELEMENT EQUATIONS AND DESCRIPTION OF THE COUPLED NUMERICAL SCHEME

The continuum is discretized into a finite element mesh. The hydrogen concentration C_L, its time derivative $\dot{C}_L$ and the hydride volume fraction f are interpolated by the standard matrix $[A]$ operating on the array of respective nodal values. Spatial derivatives of the hydrogen concentration and the hydrostatic stress are interpolated by means of the standard matrix $[B]$. Then the finite element equations are written as

$$[M]\{\dot{C}_L^N\} + [K]\{C_L^N\} = \{R\}, \tag{A.1}$$

where $[M]$ is the concentration matrix, given by

$$[M] = \int_V [A]^T Q[A]\,dV, \tag{A.2}$$

$[K]$ is the diffusivity matrix, given by

$$[K] = [K_1] + [K_2], \tag{A.3}$$

with

$$[K_1] = \int_V [B]^T D_c[B]\,dV, \tag{A.4}$$

and

$$[K_2] = -\int_V [B]^T \frac{\bar{V}_H D_c}{3RT}[B]\{\sigma_{kk}^N\}[A]\,dV, \tag{A.5}$$

$\{R\}$ is the diffusion flux vector, given by

$$\{R\} = -\int_{S_f} [A]^T \phi\,dS. \tag{A.6}$$

$\{C_L^N\}$ is the array of the nodal values of C_L, V is the volume occupied by the body, S_f is the part of the surface S where the hydrogen flux ϕ is prescribed and the symbol $[]^T$ stands for matrix transpose. The array $\{\sigma_{kk}^N\}$ contains the nodal values for σ_{kk} at each node. The parameter Q is the diffusion parameter of (9) and the parameter D_c is the effective diffusion constant defined in (10). The flux can be calculated from

$$\phi = -n_i\left(D_c C_{L,i} + \frac{D_c C_L}{RT}\mu_{\sigma,i}\right), \tag{A.7}$$

where n_i is the component of the outward unit normal vector to the surface. Evidently, equations (A.1) are nonlinear because the concentration matrix $[M]$ depends on the hydride volume fraction through the diffusion parameter Q. Also the diffusivity matrix $[K]$ depends on the effective diffusion constant D_c and the hydrostatic stresses σ_{kk} which is furnished by the elastic analysis.

The finite element equations for rate equilibrium of the solid body can be obtained directly from the principle of virtual velocities (19) and are given by

$$\int_V [B']^T\{\Delta\sigma\}\,dV = \int_S [A']^T\{\Delta T\}\,dS, \tag{A.8}$$

where $\{\Delta\sigma\} = \{\sigma\}_{t+\Delta t} - \{\sigma\}_t$ is the stress increment vector when tractions are incremented by $\{\Delta T\} = \{T\}_{t+\Delta t} - \{T\}_t$ from time t to time $t+\Delta t$, and $[A']$ and $[B']$ are the standard interpolation matrices for the velocity v_i and strain rate $\dot{\varepsilon}_{ij} = (\partial v_i/\partial x_j + \partial v_j/\partial x_i)/2$, respectively. Because the elastic moduli are assumed to be constant the stress increment vector can be written as $\{\Delta\sigma\} = [C](\{\Delta\varepsilon\} - \{\Delta\varepsilon^H\})$, where $[C]$ is the matrix of the constitutive moduli and strain increment vectors $\{\Delta\varepsilon\}$ and $\{\Delta\varepsilon^H\}$ are given in plane strain by $\{\Delta\varepsilon\}^T = [\dot{\varepsilon}_{11}\Delta t\ \dot{\varepsilon}_{22}\Delta t\ \dot{\varepsilon}_{33}\Delta t\ 2\dot{\varepsilon}_{12}\Delta t]$ and $\{\Delta\varepsilon^H\}^T = [\dot{\varepsilon}^T_{11}\Delta t\ \dot{\varepsilon}^T_{22}\Delta t\ \dot{\varepsilon}^T_{33}\Delta t\ 0]$, respectively. Therefore (A.8) can be recast into

$$\left(\int_V [B']^T[C][B']\,dA\right)\{\Delta u^N\} = \{F^N\}_{t+\Delta t} - \int_V [B']^T(\{\sigma\}_t - [C]\{\Delta\varepsilon^H\})\,dA \tag{A.9}$$

where $\{F^N\}_{t+\Delta t}$ is the nodal force vector at time $t+\Delta t$ given by

$$\{F^N\}_{t+\Delta t} = \int_S [A']^T\{T\}_{t+\Delta t}\,dS, \tag{A.10}$$

and $\{\Delta u^N\}$ is the vector of nodal displacement increments. Equations (A.10) are also nonlinear since the transformation strain increment $\{\Delta\varepsilon^H\}$ depends on the hydrogen concentration C_L and the hydride volume fraction f which in turn depend on the hydrostatic stress σ_{kk} and are furnished by the diffusion analysis.

Assuming the solution at time t has been obtained, then the displacements $\{u^N\}_t$, the hydrogen concentration $\{C^N_L\}_t$, the hydride volume fraction $\{f^N\}_t$, the hydride volume fraction rate $\{\dot{f}^N\}_t$ and the hydrostatic stress $\{\sigma^N_{kk}\}_t$ are all known at time t. Loads are then increased to a new level $\{F^N\}_{t+\Delta t}$ and the solution at time $t+\Delta t$ is to be found. Using a forward Euler method, the transformation strain increment $\{\Delta\varepsilon^H\}$ can be found from the hydride volume fraction rate $\{\dot{f}^N\}_t$. Then (A.9) can be solved for the nodal displacement increments $\{\Delta u^N\}$ and the elastic solution $\{u^N\}_{t+\Delta t} = \{u^N\}_t + \{\Delta u^N\}$ is found. This allows for the determination of the hydrostatic stress vector $\{\sigma_{kk}\}_{t+\Delta t}$. Using a modified backward Euler method (Sofronis and McMeeking, 1989) with the condition that the flux ϕ through the surface S_f is zero (no flux occurs through the axis of symmetry ahead of the crack tip), one can rewrite the diffusion equations (A.1) as

$$\left(\frac{1}{\Delta t}[M]_t + [K_1]_t\right)\{C^N_L\}_{t+\Delta t} = \left(\frac{1}{\Delta t}[M]_t - [K_2]_t\right)\{C^N_L\}_t. \tag{A.11}$$

The solution to (A.11) gives $\{C^N_L\}_{t+\Delta t}$. The hydride volume fraction $\{f^N\}_{t+\Delta t}$ is then calculated along with the readjustment of $\{C^N_L\}_{t+\Delta t}$ as described in Section 3.1. The hydride volume fraction rate $\{\dot{f}^N\}_{t+\Delta t}$ is computed as $(\{f^N\}_{t+\Delta t} - \{f^N\}_t)/\Delta t$. The solution for time $t+\Delta t$ is now complete and the procedure repeats for a further increment.